

A silver(II) route to unconventional superconductivity

Xiaoqiang Liu,^{1,*} Shishir K. Pandey,^{1,*} and Ji Feng^{1,2,3,†}

¹International Center for Quantum Materials, School of Physics, Peking University, Beijing 100871, China

²Collaborative Innovation Center of Quantum Matter, Beijing 100871, China

³CAS Center for Excellence in Topological Quantum Computation, University of Chinese Academy of Sciences, Beijing 100190, China

The highly unusual divalent silver in silver difluoride (AgF_2) features a nearly square lattice of Ag^{+2} bridged by fluorides. As a structural and electronic analogue of cuprates, its superconducting properties are yet to be examined. Our first principles electronic structure calculations reveal a striking resemblance between AgF_2 and the cuprates. Computed spin susceptibility shows a magnetic instability consistent with the experimentally observed antiferromagnetic transition. A linearized Eliashberg theory in fluctuation-exchange approximation shows an unconventional singlet d -wave superconducting pairing for bulk AgF_2 at an optimal electron doping. The pairing is found to strengthen with a decreasing interlayer coupling, highlighting the importance of quasi-2D nature of the crystal structure. These findings place AgF_2 in the category of unconventional high- T_C superconductors, and its chemical uniqueness may help shed new lights on the high- T_C phenomena.

Introduction. Superconducting properties of high T_C cuprates emerge from an intricate interplay between electronic, lattice and spin degrees of freedom [1, 2]. The cuprate crystal structure is generally derived from the perovskite type structure, featuring a few universal themes. Structurally they all contain quasi two-dimensional (2D) CuO_2 sheets. Their normal state electronic structure near the Fermi energy is dominated by a single band derived from $\text{Cu-}d$ orbitals [1–6]. In sharp contrast to conventional superconductors based on electron-phonon coupling assisted Cooper pair formation, superconductivity in cuprates is believed to be driven largely by strong electronic interactions [6]. The quasi-2D nature of crystal structure limits electronic modes in the out-of-plane direction, resulting in reduced screening and enhanced interaction that are essential to high- T_C superconductivity. Understanding obtained from the extensive studies of structural, electronic and superconducting properties of cuprates has led to discoveries of new superconducting materials [6–8]. Insights into the interplay of geometric and electronic structure are key to discovery of novel superconductors. Clearly, it is then attractive to assay materials that resemble cuprates, both structurally and electronically, for potential novel superconductivity.

Materials hosting divalent silver are extremely scarce in comparison with monovalent silver compounds. Silver difluoride (AgF_2) has been synthesized from AgNO_3 , anhydrous hydrogen fluoride treated with K_2NiF_6 and elemental fluorine, with silver ion Ag(II) in a highly unusual divalent state despite relatively large second ionization potential compares to the first one [9, 10]. More interestingly, AgF_2 resembles cuprates’s parent phase La_2CuO_4 in its geometric, electronic and magnetic structures. An AgF_2 sheet of the bulk crystal is structurally similar to a CuO_2 sheet, with similar pattern of out-of-plane displacement of anion atoms as shown in Fig. 1(a). The divalent Ag features a $3d^9$ valence shell, iso-valent to

cuprates. The antiferromagnetic ground state of charge neutral AgF_2 is a charge-transfer insulator, which again is a familiar scenario in cuprates.

It is then a natural and tempting question whether AgF_2 will turn superconducting once metallized upon doping, like the cuprates. It is therefore the purpose of this work to study whether interaction can drive a superconducting transition in AgF_2 , and what the ensuing pairing symmetry will be. We start with an investigation of crystal and electronic structure of AgF_2 and its resemblance to the archetypal cuprate, the orthorhombic La_2CuO_4 [6]. A comparison of the crystal and electronic structures obtained from first principles calculations establishes a compelling structural and electronic resemblance between these compounds. A multiband Hubbard model is constructed from which the spin susceptibility of AgF_2 within the random-phase approximation reveals an antiferromagnetic instability in accordance with experiments. Employing the fluctuation-exchange approximation and solving the linearized Eliashberg equations, we obtain the superconducting pairing strength (λ) and

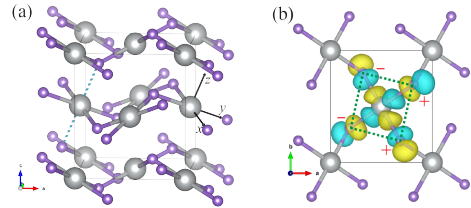


FIG. 1. (a) AgF_2 crystal structure. Purple and gray balls are F and Ag, respectively. Blue dashed lines through one of the Ag(II) indicate out-of-plane Ag-F bonds in a AgF_6 octahedron. The black arrows labeled x, y, z indicate the local coordinates used to describe d -orbitals on Ag. In (b), green dash-lined box highlights a AgF_4 unit. $+/-$ indicate out-of-plane displacements of fluoride ions. The $d_{x^2-y^2}$ Wannier orbital on the central Ag is shown.

symmetry. A phase diagram is obtained by calculating λ at various carrier doping level and Hubbard U values. The strongest superconducting pairing is obtained at 5% electron doping for bulk AgF_2 , with a dominating singlet d_{xz} symmetry. We find that the superconducting pairing strength is gradually noted to increase with decreasing interlayer coupling. We attribute this effect to the renormalization of electron-electron correlations with decreasing out-of-plane coupling.

Electronic structure. The structure of AgF_2 can be viewed as a stack of Ag-F square-planar networks resembling the cuprate planes in La_2CuO_4 [6] as shown in Fig. 1(a). Similar to the low-temperature polymorph of La_2CuO_4 [6], AgF_2 has an orthorhombic crystal structure with each Ag(II) in a distorted octahedral crystal field of six nearest-neighbor F^- ions [11, 12]. However, unlike in a perfect octahedral coordination, the out-of-plane Ag-F bonds are elongated by 24% relative to the in-plane ones as shown by blue dashed lines on one of the Ag(II) in Fig. 1(a), leaving Ag(II) 4-coordination in a AgF_2 unit. This again resembles La_2CuO_4 in which there is a 27% elongation of the out-of-plane Cu-O bonds. These four F^- -coordinated Ag(II) form AgF_4 unit within the square-planar network, as indicated by green dash-lined box in Fig. 1(b). A significant deviation of AgF_2 structure from La_2CuO_4 comes from the tilting of this AgF_4 unit by a large angle $\sim 25^\circ$, and hence the plane is puckered as shown in Fig. 1. This tilt of CuO_4 in La_2CuO_4 is much gentler ($\sim 5^\circ$). The TM-anion-TM (TM = Ag or Cu) angles in the square-planar structure are $\sim 130^\circ$ for AgF_2 , which is $\sim 173^\circ$ in La_2CuO_4 . This distortion from the ideal 180° angle is expected to manifest itself in the superexchange interaction, and therefore the temperature of magnetic ordering. Indeed, the Neél temperature (T_N) is 300 K for La_2CuO_4 and 163 K for AgF_2 [13, 14]. Given the striking similarities of structural and magnetic properties of AgF_2 with that of La_2CuO_4 and the subtle difference, investigation of its electronic properties in context of superconductivity is warranted.

As discussed earlier, a single $d_{x^2-y^2}$ orbital for AgF_2 shown in Fig. 1(b) dominating the low energy space near the Fermi level is one of the most prominent characteristic feature similar to the cuprates. This is schematically shown in Fig. 2(a) where partially filled $d_{x^2-y^2}$ shown in red, contributes at the Fermi level. In the octahedral crystal field, the d orbitals are split into a triply degenerate t_{2g} set and a doubly degenerate e_g set. Deviation from perfect octahedral symmetry described earlier lifts the degeneracy of e_g orbitals with d_{z^2} being lower in energy than the in-plane $d_{x^2-y^2}$. The occupied anion $2p$ orbitals are situated deep below the Fermi level. Non spin-polarized band structure of AgF_2 , calculated using the density-functional theory, shown in Fig. 2(b) exhibits features akin to cuprates. For calculational details, refer to the Supplemental Material(SM) [15]. The low-energy excitations are dominated by the half-filled $d_{x^2-y^2}$ on

Ag, and are well separated from all other bands. Thus when constructing a tight-binding model, it is justified to include simply one $d_{x^2-y^2}$ -like Wannier orbital per Ag. Once the Coulomb interaction is included AgF_2 becomes charge-transfer antiferromagnetic insulator similar to the cuprates in a scenario discussed also in Jakub et al [9].

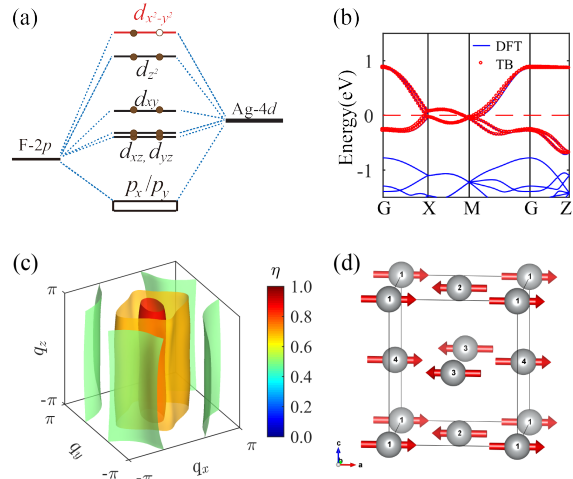


FIG. 2. (a) Schematic energy level diagram of Ag(II) in the crystal field of F atoms. (b) Non-spin polarized band structures of AgF_2 from first principles calculation (DFT) and Wannier interpolation based tight binding model (TB), near the Fermi energy. (c) $\eta(\mathbf{q})$ for undoped bulk AgF_2 with isovalue 0.5(cyan), 0.7(yellow) and 0.9(red). Here, $U=0.44$ eV and $T=14$ meV. (d) Magnetic structure of AgF_2 obtained from RPA. Red arrows represent the magnetic moment on Ag atoms.

Interaction-mediated superconductivity. To investigate the effect of interaction on the magnetic order and potential superconductivity, we construct a multiband Hubbard model,

$$H = H_0 + H_U = \sum_{ijl'l'\sigma} t_{ij}^{ll'} c_{il\sigma}^\dagger c_{j'l'\sigma} + U \sum_{il} n_{il\uparrow} n_{il\downarrow}, \quad (1)$$

where i, l and σ are lattice, orbital and spin indices, respectively, and c and n are Fermion annihilation and number operators, respectively. The low-energy bands are described by tight-binding Hamiltonian H_0 , in which hopping amplitudes are derived from the maximally-localized Wannier function approach [16] (see Table S1 in SM [15]). The resultant band structure is shown in Fig. 2(b), where the four $d_{x^2-y^2}$ bands (four Ag per unit cell) from the tight-binding model fit the first principles bands well. The intra-orbital Hubbard parameter U is determined by estimating the Neél temperature in a random-phase approximation (RPA), as described next.

Within the RPA [17–21], the charge (χ^c) and spin (χ^s) susceptibilities are given by,

$$\begin{aligned} \chi^c(\mathbf{q}) &= [1 + \chi^0(\mathbf{q})U^c]^{-1} \chi^0(\mathbf{q}), \\ \chi^s(\mathbf{q}) &= [1 - \chi^0(\mathbf{q})U^s]^{-1} \chi^0(\mathbf{q}), \end{aligned} \quad (2)$$

where $q = (\mathbf{q}, \omega)$, χ^0 is the bare susceptibility, and U^c and U^s are the interaction matrices in the charge and spin channels, respectively [15]. The onset of spin instability is detected by the condition $|1 - \chi_0(\mathbf{q}, 0)U^s| = 0$, which happens when the maximum eigenvalue of $\chi_0(\mathbf{q}, 0)U^s$ (denoted by $\eta(\mathbf{q})$) becomes unity at any \mathbf{q} . The ensuing divergence of χ^s leads to a magnetic phase transition. The vector \mathbf{q}^* and temperature T_N at which $\eta(\mathbf{q}^*) = 1$ are the Néel temperature and propagation vector of the spin pattern, respectively. The spin pattern corresponding to a \mathbf{q}^* is determined by diagonal elements of the eigenvector $\xi(\mathbf{q}^*)$ corresponding to $\eta(\mathbf{q}^*)$. We use a mesh of $48 \times 48 \times 48$ for Brillouin zone sampling in all our calculations on the Hubbard model.

The Hubbard U is estimated to be 0.44 eV, by matching the experimentally observed Néel temperature (~ 163 K) of AgF_2 (Fig. S1 in SM [15]). Isosurfaces of $\eta(\mathbf{q})$ drawn in Fig. 2(a) for undoped bulk AgF_2 at $T = 14$ meV (~ 163 K) show a strong anisotropy corresponding to a strong intra-layer and a weak interlayer magnetic exchange interactions. Henceforth, we focus on $q_z = 0$ plane in current analysis. The maximum value of $\eta(\mathbf{q})$ is found to lie along the q_z -axis. Thus, for a weak interlayer coupling when restricted only in the q_x - q_y plane, the maximum value of the spin susceptibility is attained at $\mathbf{q} = 0$. The computed eigenvectors $\xi_{ll}(\mathbf{q} = 0)$ yield an antiferromagnetic order shown in Fig. 2(d), consistent with the experimentally established Néel state in AgF_2 [14].

When doped with a carrier concentration that readily suppresses the magnetism, a cuprate goes metallic exhibiting various kind of instability such as charge and spin fluctuations at low temperatures due to Fermi surface reconstruction. The Hubbard models have been used extensively to explain the superconductivity in doped cuprates [7]. Keeping the striking resemblance of AgF_2 with cuprates, similar approach of metallization by carrier doping applies in AgF_2 as well. Thus, having a model capable of describing the magnetic instability and order of AgF_2 , we go on to a scrutiny for potential superconductivity mediated by spin fluctuation. The fluctuation-exchange approximation (FLEX) [22, 23] is employed to describe the effective electron-electron interaction $\Gamma(q)$ given by,

$$\Gamma(q) = \gamma U^s \chi^s(q) U^s - \frac{1}{2} U^c \chi^c(q) U^c + \frac{1}{2} (U^s + U^c) \quad (3)$$

with $\gamma = \frac{3}{2}$ for the singlet channel and $\gamma = -\frac{1}{2}$ for the triplet channel. An effective pairing between the electrons on the Fermi surface arising from spin and/or charge fluctuations can result in the formation of Cooper pairs. To describe the pairing instability of this type, the linearized Eliashberg equation is solved in the weak-coupling regime,

$$\lambda \phi_{mn}(\mathbf{k}) = -\frac{1}{N} \sum_{\mathbf{k}'} \sum_{\mu\nu} \Gamma_{\mu\nu}^{mn}(\mathbf{k}, \mathbf{k}') F_{\mu\nu}(\mathbf{k}') \phi_{\mu\nu}(\mathbf{k}') \quad (4)$$

where $F_{\mu\nu}(\mathbf{k}')$ is a factor arising from summing the product of Green's functions over Matsubara frequencies and m, n, μ, ν are band indices. $\phi_{mn}(\mathbf{k})$ is the order parameter of superconducting phase [15]. Eq.(4) then is an eigenvalue equation. The largest eigenvalue λ_{\max} becomes unity at superconducting T_C and can be used to gauge the relative pairing strength near the T_C .

Eq.(4) is solved for various doping levels and U values at $T = 30$ meV. Fig. 3(a) shows the contour plot for λ_{\max} in the $U - \delta n$ parameter space. As observed in Fig. 3(a) the superconducting pairing strength increases with increasing U at a given doping, underlining the importance of electronic correlation for potential superconductivity in this compound. The symmetry of pairing can be identified by assigning each solved $\phi_{mn}(\mathbf{k})$ to an irreducible representation of the D_{2h} point group, symmetry group of the bulk AgF_2 . Corresponding to each irreducible representation i (Table S2 in SM [15]), the largest eigenvalue is denoted by λ_{\max}^i . Fig. 3(b) shows the doping dependence of λ_{\max}^i for various pairing symmetry at $U = 0.44$ eV. One can find that the singlet d -wave pairings have significantly higher strength than triplet p -wave pairings and the leading pairing symmetry is singlet d_{xz} -type wave throughout the $U - \delta n$ parameter space shown in Fig. 3(a). Moreover, the hole doping readily decreases λ , while the electron doping tends to increase λ at first, reaching a peak value at an optimal doping of 5% beyond which further doping tends to reduce λ .

To circumvent the gauge problem [15] of $\phi_{mn}(\mathbf{k})$ for degenerate bands, we define $\phi(\mathbf{k})$ as

$$\phi(\mathbf{k}) = \sum_n \phi_{nn}(\mathbf{k}) \delta(\varepsilon_{n\mathbf{k}} - \varepsilon_F) \quad (5)$$

which describes the nature of order parameter on Fermi surface. Here $\varepsilon_{n\mathbf{k}}$ and ε_F are band energy and Fermi energy respectively. Energy cutoff of 5 meV is considered for evaluation of δ function in our calculations. We plot the real part of $\phi(\mathbf{k})$ corresponding to λ_{\max} for one of the AgF_2 layers with $U = 0.44$ eV and optimal doping of 5%. This is shown in Fig. 3(c) in the 3-dimensional Brillouin zone, and Fig. 3(d) shows a projection onto the k_x - k_z plane. One encounters nodes crossing $k_x = \pi$ or $k_z = \pi$ planes indicating a d_{xz} -wave pairing. Hence, it can be concluded that the bulk AgF_2 crystal becomes unstable to a d -wave pairing induced by spin fluctuation.

Interlayer coupling. As discussed in the beginning, quasi-2D nature of the crystal structure of cuprates is one of the factors favoring its high T_C [24, 25]. In the case of AgF_2 , although Ag-F layers resemble the copper oxide sheets, the separation of these planes is 2.91 Å, much smaller than what is observed for La_2CuO_4 (6.6 Å) as well as other cuprates. Consequently, the effect of interlayer coupling on superconducting properties of AgF_2 clearly warrants further study. In other words, AgF_2 provides a good platform to investigate the role of

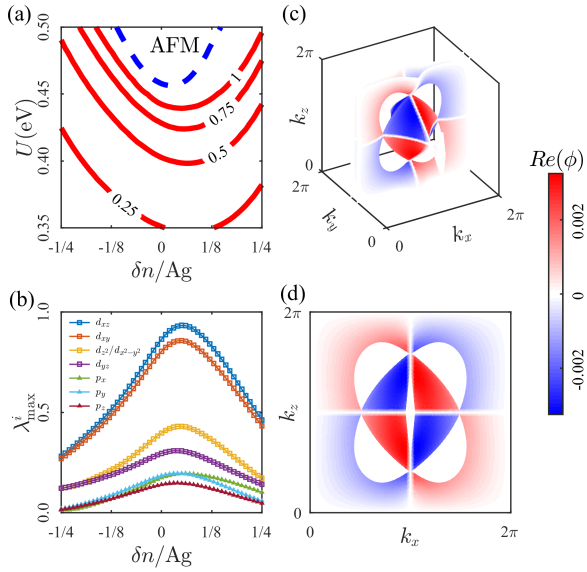


FIG. 3. (a) Contour plot of λ_{\max} of the linearized Eliashberg equation at $T = 30$ meV. Blue dash line correspond to $\eta(\mathbf{q})$ reach to unity at any \mathbf{q} . (b) Doping dependence of λ_{\max}^i for several pairing symmetry of bulk AgF_2 at $U = 0.44$ eV and $T = 30$ meV. Square representing the singlet and triangle representing the triplet channels. (c) Three-dimensional and (d) projection on k_x - k_z plane, of the order parameter $\phi(\mathbf{k})$ at Fermi surface of one of the AgF_2 layer with $\delta n/\text{Ag} = 0.05$ for bulk AgF_2 .

quasi-2D nature of crystal structure in superconducting properties. Additionally, monolayer or few-layer samples more prone to doping by techniques such as field or electrolytic gating [26], which is a clear experimental advantage.

To study the effect of interlayer coupling on superconducting properties of AgF_2 , we interpolate between the bulk and monolayer limits as follow,

$$H_0 = H^{\text{intra}} + \alpha H^{\text{inter}} \quad (6)$$

Here, H^{intra} is a tight binding model within a single layer of AgF_2 , while H^{inter} is the interlayer hopping term, which is scaled by $\alpha \in [0, 1]$. Bulk AgF_2 can be obtained with $\alpha = 1$, and $\alpha = 0$ correspond to a single layer of AgF_2 [27].

In Fig. 4(a), $\lambda_{\max}^{d_{xy}}$ and $\lambda_{\max}^{d_{xz}}$ as functions of doping concentrations for different interlayer coupling strength α are shown. It can be seen that the interlayer coupling tends to suppress the superconducting pairing in both hole and electron doping because a stronger interlayer coupling amounts to a weaker electronic correlations as discussed earlier. Evidently the quasi-2D nature of the crystal structure is one of the crucial factors in the favor of high T_C superconductivity, which again confirms the resemblance to cuprates. The optimal electron doping concentration remains unchanged as of bulk AgF_2 , which

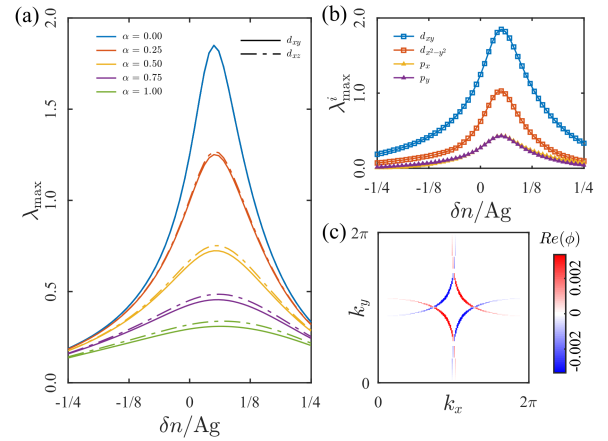


FIG. 4. (a) Doping dependence of $\lambda_{\max}^{d_{xy}}$ and $\lambda_{\max}^{d_{xz}}$ for different interlayer coupling α at $U = 0.37$ eV and $T = 30$ meV. (b) Doping dependence of λ_{\max}^i of various pairing symmetry in single layer AgF_2 . (c) Plot of order parameter $\phi(\mathbf{k})$ in k_x - k_y plane at Fermi surface in single layer AgF_2 with $\delta n/\text{Ag} = 0.05$.

indicates that the Fermi surface nesting responsible for divergence of spin susceptibility mainly occur within a single layer without any significant interlayer contribution. In the absence of interlayer coupling, the separated monolayers have the same leading pairing symmetry of the d_{xy} -type. These two degenerate d_{xy} wave then split into d_{xz} and d_{xy} immediately after the interlayer coupling was switched on. The difference of pairing strength between leading d_{xz} wave and competing d_{xy} was also found to increase with increase of α .

For single layer AgF_2 , the symmetry reduces to C_{2h} point group from D_{2h} of bulk AgF_2 . Performing similar analysis to that for bulk, we show the doping dependence of λ_{\max}^i for several pairing symmetry for single layer in Fig. 4(b). As seen previously in Fig. 4(a), the leading pairing symmetry is d_{xy} followed by $d_{x^2-y^2}$ wave. The real part of the $\phi(\mathbf{k})$ corresponding to the λ_{\max} at the optimal doping concentration is shown in Fig. 4(c), which clearly reveals d_{xy} pairing symmetry in the monolayer limit.

Summary and outlook. Our calculations indicate AgF_2 is not only chemically exotic, but also harbors unconventional superconductivity in a way very similar to high- T_C cuprates. Our multiband Hubbard model reveals a magnetic instability in accordance with the experimentally obtained magnetic ground state. In the fluctuation-exchange approximation, we find a superconducting ground state with a singlet d -wave pairing for the bulk AgF_2 at an optimal electron doping of 5%. By varying the strength of interlayer interaction, we show that the superconducting pairing strength increases with decreasing interlayer coupling, highlighting the crucial role played by quasi-2D crystal structure on superconducting properties of such materials.

Drawing hints from cuprates, metallization of bulk AgF_2 can be achieved by synthesizing it with a modified composition as is done in case of $\text{La}_{2-x}\text{Ba}_x\text{CuO}_4/\text{La}_{2-x}\text{Sr}_x\text{CuO}_4$ [1, 28], leading to doping of extra charge carriers in transition metal-anion plane. Another route to metallization is electric gating [29]. A monolayer of AgF_2 may be realized by epitaxial growth [30], metallization of which can be achieved during the deposition process. The idea of liquid-gating induced superconductivity in thin films [31] can also be applied to monolayer AgF_2 .

This work is supported by the National Natural Science Foundation of China (Grant No. 11725415 and No. 11934001), the Ministry of Science and Technology of China (Grant No. 2018YFA0305601 and No. 2016YFA0301004), and the Strategic Priority Research Program of the Chinese Academy of Sciences (Grant No. XDB28000000).

* Equal contribution

† jfeng11@pku.edu.cn

- [1] J. G. Bednorz and K. A. Müller, *Z. Phys. B - Cond. Mat.* **64**, 189 (1986).
- [2] J. G. Bednorz, M. Takashige, and K. A. Müller, *Europhysics Letters (EPL)* **3**, 379 (1987).
- [3] J. G. Bednorz and K. A. Müller, *Rev. Mod. Phys.* **60**, 585 (1988).
- [4] E. Dagotto, *Rev. Mod. Phys.* **66**, 763 (1994).
- [5] M. A. Kastner, R. J. Birgeneau, G. Shirane, and Y. Endoh, *Rev. Mod. Phys.* **70**, 897 (1998).
- [6] D. J. Scalapino, *Rev. Mod. Phys.* **84**, 1383 (2012).
- [7] G. R. Stewart, *Rev. Mod. Phys.* **83**, 1589 (2011).
- [8] Y. Cao, V. Fatemi, S. Fang, K. Watanabe, T. Taniguchi, E. Kaxiras, and P. Jarillo-Herrero, *Nature* **556**, 43 (2018).
- [9] J. Gawraczyński, D. Kurzydłowski, R. A. Ewings, S. Bandaru, W. Gadomski, Z. Mazej, G. Ruani, I. Bergenti, T. Jaroń, A. Ozarowski, S. Hill, P. J. Leszczyński, K. Tokár, M. Derzsi, P. Barone, K. Wohlfeld, J. Lorenzana, and W. Grochala, *Proc. Natl. Acad. Sci. USA* **116**, 1495 (2019).
- [10] C. Miller and A. S. Botana, *Phys. Rev. B* **101**, 195116 (2020).
- [11] P. Charpin, P. Plurien, and P. Meriel, *Bull. Soc. Fr. Miner. Cristallogr.* **93**, 7 (1970).
- [12] P. Fischer, D. Schwarzenbach, and H. Rietveld, *J. Phys. Chem. Solids* **32**, 543 (1971).
- [13] N. P. Armitage, P. Fournier, and R. L. Greene, *Rev. Mod. Phys.* **82**, 2421 (2010).
- [14] P. Fischer, G. Roullet, and D. Schwarzenbach, *J. Phys. Chem. Solids* **32**, 1641 (1971).
- [15] See Supplemental Material at XXX for details about the methodology of *ab initio*, random-phase approximation and fluctuation exchange approximation calculations, character table for D_{2h} and C_{2h} point group symmetry and Fig. S1.
- [16] A. A. Mostofi, J. R. Yates, Y.-S. Lee, I. Souza, D. Vanderbilt, and N. Marzari, *Comput. Phys. Commun.* **178**, 685 (2008).
- [17] S. Graser, T. A. Maier, P. J. Hirschfeld, and D. J. Scalapino, *New J. Phys.* **11**, 025016 (2009).
- [18] T. A. Maier, S. Graser, P. J. Hirschfeld, and D. J. Scalapino, *Phys. Rev. B* **83**, 100515 (2011).
- [19] K. Kuroki, S. Onari, R. Arita, H. Usui, Y. Tanaka, H. Kontani, and H. Aoki, *Phys. Rev. Lett.* **101**, 087004 (2008).
- [20] X. Wu, F. Yang, C. Le, H. Fan, and J. Hu, *Phys. Rev. B* **92**, 104511 (2015).
- [21] K. Kuroki, H. Usui, S. Onari, R. Arita, and H. Aoki, *Phys. Rev. B* **79**, 224511 (2009).
- [22] N. E. Bickers, D. J. Scalapino, and S. R. White, *Phys. Rev. Lett.* **62**, 961 (1989).
- [23] T. Takimoto, T. Hotta, and K. Ueda, *Phys. Rev. B* **69**, 104504 (2004).
- [24] D. Jiang, T. Hu, L. You, Q. Li, A. Li, H. Wang, G. Mu, Z. Chen, H. Zhang, G. Yu, J. Zhu, Q. Sun, C. Lin, H. Xiao, X. Xie, and M. Jiang, *Nat. Commun.* **5**, 5708 (2014).
- [25] Y. Yu, L. Ma, P. Cai, R. Zhong, C. Ye, J. Shen, G. D. Gu, X. H. Chen, and Y. Zhang, *Nature* **575**, 156 (2019).
- [26] J. T. Ye, Y. J. Zhang, R. Akashi, M. S. Bahramy, R. Arita, and Y. Iwasa, *Science* **338**, 1193 (2012).
- [27] A Hubbard $U = 0.37$ eV is used for the monolayer calculation, as the reduced screening leads to divergent susceptibility if the bulk U value is used. The results here only show the qualitative trend.
- [28] A. T. Bollinger, G. Dubuis, J. Yoon, D. Pavuna, J. Misewich, and I. Božović, *Nature* **472**, 458 (2011).
- [29] A. Goldman, *Annu. Rev. Mater. Res.* **44**, 45 (2014).
- [30] A. Grzelak, H. Su, X. Yang, D. Kurzydłowski, J. Lorenzana, and W. Grochala, *Phys. Rev. Materials* **4**, 084405 (2020).
- [31] J. T. Ye, S. Inoue, K. Kobayashi, Y. Kasahara, H. T. Yuan, H. Shimotani, and Y. Iwasa, *Nature Materials* **9**, 125 (2010).

Supplemental Material:

A silver(II) route to unconventional superconductivity

Xiaoqiang Liu,^{1,*} Shishir K. Pandey,^{1,*} and Ji Feng^{1,2,3,†}

¹*International Center for Quantum Materials,*

School of Physics, Peking University, Beijing 100871, China

²*Collaborative Innovation Center of Quantum Matter, Beijing 100871, China*

³*CAS Center for Excellence in Topological Quantum Computation,
University of Chinese Academy of Sciences, Beijing 100190, China*

A. Density-functional theory calculations

To calculate electronic structure of AgF_2 , we have performed density-functional theory based calculations using Vienna *ab initio* simulation package(VASP) [1]. The projector-augmented wave potentials are used in our calculations [2, 3], with a $6 \times 6 \times 8$ Gamma-centered mesh of k-points and a plane wave cutoff of 800 eV. The results are found to be well converged with respect to k-point mesh and plane wave numbers. The Perdew-Burke-Ernzerhof functional [4] is used for the exchange-correlation functional, and additional electron-electron correlation is included statically by a $U = 8$ eV within the GGA+U formalism [5]. The total energy is calculated self-consistently till the energy difference between successive steps is below 10^{-5} eV. The experimental lattice parameters of orthorhombic AgF_2 with space group $Pbca$ (No. 61) are $-\mathbf{a}- = 5.101 \text{ \AA}$, $-\mathbf{b}- = 5.568 \text{ \AA}$ and $-\mathbf{c}- = 5.831 \text{ \AA}$ [6].

Considering the experimentally observed magnetic ground state and $U = 8$ eV on Ag- d states, we perform full optimization of lattice parameters. The value of U on Ag- d orbital is chosen to match the experimentally observed Ag magnetic moments of $0.7 \mu_B/\text{Ag}$. Change in \mathbf{a} and \mathbf{b} lattice constants were found to be less than 1 % while the \mathbf{c} vector was enhanced by $\sim 1.7\%$. Since these values are very close to the experimental ones, we use the experimental structure for further study. Non-spin polarized *ab initio* band structure was projected onto a tight-binding model using the maximally-localized Wannier functions for the radial part of the wavefunctions using WANNIER90-VASP interface, implemented within VASP [7]. Mapping is done for the undoped case considering Ag- $d_{x^2-y^2}$ orbitals and the hopping amplitudes are listed in Table S1.

B. Random-phase approximation and fluctuation exchange approximation

We start by setting up the multiband Hubbard model, by adding the Hubbard U term to a tight-binding model described in section A,

$$H = H^{\text{TB}} + H^{\text{hub}} = \sum_{ijl'l'\sigma} t_{ij}^{ll'} c_{il\sigma}^\dagger c_{jl'\sigma} + U \sum_{il} n_{il\uparrow} n_{il\downarrow} \quad (1)$$

Here, $c_{il\sigma}$ is annihilation operator of $d_{x^2-y^2}$ orbital on Ag site l in i^{th} unit cell with spin σ and $t_{ij}^{ll'}$ is hopping amplitude. U is the on-site Hubbard parameter.

The random-phase approximation(RPA) [8–12] is employed to study the magnetic insta-

TABLE S1. List of all hopping amplitudes larger than 5 meV in our Wannier function based tight-binding model of bulk AgF₂. \mathbf{R} and l/l' are the translation vector and orbital index respectively. All other hoppings not listed here can be obtained by applying symmetry operations of $Pbca$, the space group of bulk AgF₂.

\mathbf{R}	l	l'	t (meV)
(0, 0, 0)	1	2	-173.1
(1, -1, 0)	1	1	34.4
(0, 1, 0)	1	1	34.0
(0, 1, -1)	1	1	28.0
(0, -1, 0)	1	3	22.8
(0, 0, -1)	1	2	18.2
(1, 0, -1)	1	1	18.1
(1, 1, 0)	1	1	15.1
(0, 1, 0)	1	3	-11.4
(0, 0, 0)	1	4	7.8
(1, 0, 1)	1	1	7.1
(0, 0, 0)	1	3	-7.0
(1, 0, 0)	1	4	-6.1
(1, -1, -1)	1	1	-5.6
(1, 0, 0)	1	3	5.3
(1, 0, 0)	1	1	5.1

bility of the system. The RPA spin and charge susceptibilities are given by

$$\begin{aligned}\chi^c(q) &= [1 + \chi^0(q)U^c]^{-1} \chi^0(q) \\ \chi^s(q) &= [1 - \chi^0(q)U^s]^{-1} \chi^0(q)\end{aligned}\tag{2}$$

respectively, where

$$(U^{c/s})_{l_3 l_4}^{l_1 l_2} = \begin{cases} U & l_1 = l_2 = l_3 = l_4 \\ 0 & \text{otherwise} \end{cases}.\tag{3}$$

Here $q = (\mathbf{q}, \omega)$.

In above expression the bare susceptibility $\chi^0(q)$ is given by,

$$(\chi^0)_{l_3 l_4}^{l_1 l_2}(\mathbf{q}, \omega) = -\frac{1}{N} \sum_{\mathbf{k}, \mu\nu} \frac{a_\nu^{l_2}(\mathbf{k} + \mathbf{q}) a_\nu^{l_3*}(\mathbf{k} + \mathbf{q}) a_\mu^{l_4}(\mathbf{k}) a_\mu^{l_1*}(\mathbf{k})}{\omega + \varepsilon_{\mu\mathbf{k}} - \varepsilon_{\nu\mathbf{k}+\mathbf{q}} + i0^+} [f(\varepsilon_{\mu\mathbf{k}} - \varepsilon_F) - f(\varepsilon_{\nu\mathbf{k}+\mathbf{q}} - \varepsilon_F)], \quad (4)$$

where N is the number of \mathbf{k} -points and μ, ν are the band indices. $a_\mu^l(\mathbf{k})$ is the l component of wave function of band μ , obtained from diagonalization of H^{TB} and $\varepsilon_\mu(\mathbf{k})$ is the corresponding eigenvalues of band μ at \mathbf{k} -point. $f(E)$ is the Fermi-Dirac distribution and ε_F is Fermi energy.

Under fluctuation exchange approximation(FLEX) [13, 14], the pairing vertex describing the effective electron-electron interaction is given by,

$$\Gamma(q) = \gamma U^s \chi^s(q) U^s - \frac{1}{2} U^c \chi^c(q) U^c + \frac{1}{2} (U^s + U^c), \quad (5)$$

with $\gamma = \frac{3}{2}$ for the singlet channel and $\gamma = -\frac{1}{2}$ for the triplet channel. The singlet vertex is symmetrized as,

$$(\Gamma^s)_{l_3 l_4}^{l_1 l_2}(k, k') = \frac{1}{2} \left((\Gamma^s)_{l_3 l_4}^{l_1 l_2}(k, k') + (\Gamma^s)_{l_3 l_2}^{l_1 l_4}(k, -k') \right), \quad (6)$$

and the triplet vertex is anti-symmetrized as,

$$(\Gamma^t)_{l_3 l_4}^{l_1 l_2}(k, k') = \frac{1}{2} \left((\Gamma^t)_{l_3 l_4}^{l_1 l_2}(k, k') - (\Gamma^t)_{l_3 l_2}^{l_1 l_4}(k, -k') \right), \quad (7)$$

Here, $\Gamma(k, k') = \Gamma(q)$ with $q = k - k'$.

The linearized Eliashberg equation will then be solved to obtain the order parameter and superconducting transition temperature,

$$\lambda \phi_{l_1 l_3}(k) = -\frac{T}{N} \sum_q \sum_{l_2 l_4 l_5 l_6} \Gamma_{l_3 l_4}^{l_1 l_2}(q) \phi_{l_5 l_6}(k - q) G_{l_2 l_5}(k - q) G_{l_4 l_6}(q - k). \quad (8)$$

Here, λ is the eigenvalue indicating the pairing strength. The eigenvector $\phi_{l_1 l_2}(k)$ is the order parameter written in term of orbital index l_1 and l_2 . $G_{l_1 l_2}(k)$ is the Matsubara Green function.

In the weak-coupling regime, the pairing vertex is approximated to be frequency-independent i.e. $\Gamma(q) = \Gamma(\mathbf{q}, \omega = 0)$. After summing over the Matsubara frequencies, we obtain the following equation in band basis,

$$\lambda \phi_{mn}(\mathbf{k}) = -\frac{1}{N} \sum_{\mathbf{k}'} \sum_{\mu\nu} (\Gamma^\eta)_{\mu\nu}^{mn}(\mathbf{k}, \mathbf{k}') F_{\mu\nu}(\mathbf{k}') \phi_{\mu\nu}(\mathbf{k}'), \quad (9)$$

where

$$F_{\mu\nu}(\mathbf{k}) = -\frac{f(\varepsilon_{\mu\mathbf{k}} - \varepsilon_F) + f(\varepsilon_{\nu-\mathbf{k}} - \varepsilon_F) - 1}{\varepsilon_{\mu\mathbf{k}} + \varepsilon_{\nu-\mathbf{k}} - 2\varepsilon_F}. \quad (10)$$

The transformation between orbital basis and band basis for the order parameter is

$$\phi_{mn}(\mathbf{k}) = \sum_{l_1 l_2} \phi_{l_1 l_2}(\mathbf{k}) a_m^{l_1*}(\mathbf{k}) a_n^{l_2*}(-\mathbf{k}), \quad (11)$$

and for the vertex,

$$(\Gamma^\eta)_{\mu\nu}^{mn}(\mathbf{k}, \mathbf{k}') = \sum_{l_1 l_2 l_3 l_4} a_m^{l_1*}(\mathbf{k}) a_n^{l_3*}(-\mathbf{k}) (\Gamma^\eta)_{l_3 l_4}^{l_1 l_2}(\mathbf{k} - \mathbf{k}') a_\mu^{l_2}(\mathbf{k}') a_\nu^{l_4}(-\mathbf{k}'). \quad (12)$$

C. Pairing symmetry

One can see that $\phi_{mn}(\mathbf{k})$ is not gauge invariant because of the eigenvector $a_\mu^l(\mathbf{k})$ involved in Eq.(11). However, if the following gauge is chosen,

$$a_n^l(-\mathbf{k}) = a_n^l(\mathbf{k})^* \quad (13)$$

for the non-magnetic state [15], then the trace of $\phi_{mn}(\mathbf{k})$

$$\phi(\mathbf{k}) = \sum_n \phi_{nn}(\mathbf{k}) \quad (14)$$

or trace taken on Fermi surface

$$\phi(\mathbf{k}) = \sum_n \phi_{nn}(\mathbf{k}) \delta(\varepsilon_{n\mathbf{k}} - \varepsilon_F) \quad (15)$$

is gauge invariant.

For the symmetry group of normal state Hamiltonian H , which are D_{2h} for bulk AgF_2 and C_{2h} for single layer AgF_2 , $\phi(\mathbf{k})$ can be identified as one of the irreducible representations of the symmetry group. All the irreducible representation and basis functions of D_{2h} are listed in Table S2 and C_{2h} in Table S3. Note that the C_2 rotation in C_{2h} is along x -axis.

TABLE S2. Character table for D_{2h} point group

	E	$C_2(z)$	$C_2(y)$	$C_2(x)$	i	$\sigma(xy)$	$\sigma(xz)$	$\sigma(yz)$	Linear, Rotations	Quadratic
A_g	+1	+1	+1	+1	+1	+1	+1	+1	—	$x^2 - y^2, z^2$
B_{1g}	+1	+1	-1	-1	+1	+1	-1	-1	R_z	xy
B_{2g}	+1	-1	+1	-1	+1	-1	+1	-1	R_y	xz
B_{3g}	+1	-1	-1	+1	+1	-1	-1	+1	R_x	yz
A_u	+1	+1	+1	+1	-1	-1	-1	-1	—	—
B_{1u}	+1	+1	-1	-1	-1	-1	+1	+1	z	—
B_{2u}	+1	-1	+1	-1	-1	+1	-1	+1	y	—
B_{3u}	+1	-1	-1	+1	-1	+1	+1	-1	x	—

 TABLE S3. Character table for C_{2h} point group

	E	$C_2(x)$	i	σ_h	Linear, Rotations	Quadratic
A_g	+1	+1	+1	+1	R_x	$x^2 - y^2, z^2, yz$
B_{1g}	+1	-1	+1	-1	R_y, R_z	xy, xz
A_u	+1	+1	-1	-1	x	—
B_{1u}	+1	-1	-1	+1	y, z	—

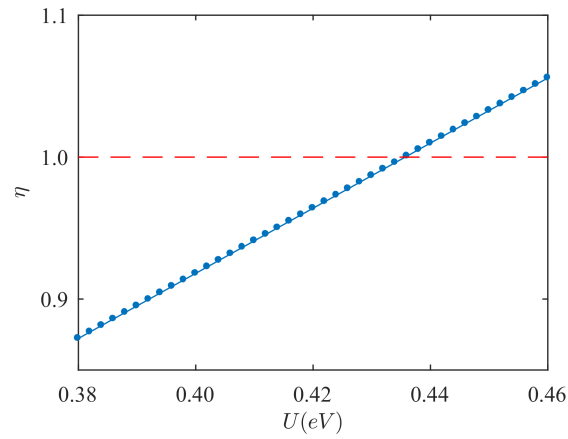


FIG. S1. The U dependence of largest η at experimental Néel temperature (~ 163 K = 14 meV). $\eta \approx 1$ when $U = 0.44$ eV.

* Equal contribution

† jfeng11@pku.edu.cn

- [1] G. Kresse and J. Furthmüller, *Phys. Rev. B* **54**, 11169 (1996).
- [2] G. Kresse and D. Joubert, *Phys. Rev. B* **59**, 1758 (1999).
- [3] P. E. Blöchl, *Phys. Rev. B* **50**, 17953 (1994).
- [4] J. P. Perdew, K. Burke, and M. Ernzerhof, *Phys. Rev. Lett.* **77**, 3865 (1996).
- [5] S. L. Dudarev, G. A. Botton, S. Y. Savrasov, C. J. Humphreys, and A. P. Sutton, *Phys. Rev. B* **57**, 1505 (1998).
- [6] P. Charpin, P. Plurien, and P. Meriel, *Bull. Soc. Fr. Miner. Cristallogr.* **93**, 7 (1970).
- [7] A. A. Mostofi, J. R. Yates, Y.-S. Lee, I. Souza, D. Vanderbilt, and N. Marzari, *Comput. Phys. Commun.* **178**, 685 (2008).
- [8] S. Graser, T. A. Maier, P. J. Hirschfeld, and D. J. Scalapino, *New J. Phys.* **11**, 025016 (2009).
- [9] T. A. Maier, S. Graser, P. J. Hirschfeld, and D. J. Scalapino, *Phys. Rev. B* **83**, 100515 (2011).
- [10] K. Kuroki, S. Onari, R. Arita, H. Usui, Y. Tanaka, H. Kontani, and H. Aoki, *Phys. Rev. Lett.* **101**, 087004 (2008).
- [11] X. Wu, F. Yang, C. Le, H. Fan, and J. Hu, *Phys. Rev. B* **92**, 104511 (2015).
- [12] K. Kuroki, H. Usui, S. Onari, R. Arita, and H. Aoki, *Phys. Rev. B* **79**, 224511 (2009).
- [13] N. E. Bickers, D. J. Scalapino, and S. R. White, *Phys. Rev. Lett.* **62**, 961 (1989).
- [14] T. Takimoto, T. Hotta, and K. Ueda, *Phys. Rev. B* **69**, 104504 (2004).
- [15] A. F. Kemper, T. A. Maier, S. Graser, H.-P. Cheng, P. J. Hirschfeld, and D. J. Scalapino, *New J. Phys.* **12**, 073030 (2010).